APPLIED SCIENCES AND ENGINEERING

GLUT4-overexpressing engineered muscle constructs as a therapeutic platform to normalize glycemia in diabetic mice

Margarita Beckerman[1,2], Chava Harel[3,2], Inbal Michael[1], Amira Klip[4], Philip J. Bilan[4], Emily J. Gallagher[5], Derek LeRoith[5], Eli C. Lewis[6], Eddy Karnieli[3,2], Shulamit Levenberg[1,2]*

Skeletal muscle insulin resistance is a main defect in type 2 diabetes (T2D), which is associated with impaired function and content of glucose transporter type 4 (GLUT4). GLUT4 overexpression in skeletal muscle tissue can improve glucose homeostasis. Therefore, we created an engineered muscle construct (EMC) composed of GLUT4-overexpressing (OEG4) cells. The ability of the engineered implants to reduce fasting glucose levels was tested in diet-induced obesity mice. Decrease and stabilization of basal glucose levels were apparent up to 4 months after implantation. Analysis of the retrieved constructs showed elevated expression of myokines and proteins related to metabolic processes. In addition, we validated the efficiency of OEG4-EMCs in insulin-resistant mice. Following high glucose load administration, mice showed improved glucose tolerance. Our data indicate that OEG4-EMC implant is an efficient mode for restoring insulin sensitivity and improving glucose homeostasis in diabetic mice. Such procedure is a potential innovative modality for T2D therapy.

INTRODUCTION

Skeletal muscle tissue takes part in various functions in the body. It comprises about 40% of total body weight and provides stability and movement to the skeleton (*1*). Skeletal muscle also plays a major role in glucose homeostasis, glycogen and lipid metabolism, and more. In recent years, the skeletal muscle tissue has been identified as a secretory organ; upon contraction, it releases muscle-specific cytokines and myokines that have local and/or systemic effects (*2*–*4*). The skeletal muscle tissue is responsible for about 80% of infused glucose uptake (*5*). Skeletal muscle insulin resistance is a key defect in type 2 diabetes (T2D) and obesity (*5*–*7*). The clinical guideline for T2D treatment is to normalize glycemia and thus minimize the chronic diabetes–related complications that can lead to medical disability, reduction in life expectancy, and high health costs (*8*, *9*). The treatment consists of lifestyle modification and various oral and injectable pharmaceutical agents. The commonly used drugs mainly aim to stimulate insulin secretion, reduce hepatic glucose production, modulate incretin levels, and inhibit sodium-glucose co-transporter-2 activity. Specific agents for improving insulin action, such as peroxisome proliferator–activated receptor γ agonists, are scarcely used (*7*, *10*, *11*). Despite numerous treatment options, patients often fail to achieve target glycemic values (*8*, *12*). To improve the overall patient health, there is a need for developing long-acting, stimuli-responsive, and alternate delivery systems (*13*–*17*).

Insulin resistance is a main clinical feature of T2D; hence, enhancing insulin sensitivity is a valid therapeutic target. Upon insulin stimulation, glucose uptake is mediated through the adipose- and muscle-specific insulin-responsive glucose transporter type 4 (GLUT4) (*18*–*20*). GLUT4 has a very long half-life of over 24 hours (*21*) and a slow recycling rate allowing high availability upon a response to insulin stimuli (*20*).

One of the prominent defects detected in T2D is impaired GLUT4 translocation machinery and a reduction of GLUT4 cellular levels (*20*, *22*–*25*). Studies in GLUT4 transgenic (TG) and knockout animals have provided important insights; the modified expression of GLUT4 in these animals, either systemic (*26*–*31*) or muscle tissue specific (*32*–*35*), influenced whole-body insulin action and glucose metabolism. GLUT4 knockout mice exhibited insulin resistance and glucose intolerance and developed a diabetic phenotype (*30*, *34*, *35*). Mice overexpressing GLUT4 showed improved insulin action and reduced glycemic levels at both fasting and postprandial states (*26*–*29*, *31*–*33*).

Following these findings and the potential of GLUT4 to normalize glycemic values, we propose an alternative innovative therapeutic platform based on tissue engineering. Skeletal muscle engineering offers a potential solution for muscle regeneration following muscle loss due to trauma or diseases (*36*, *37*). In recent years, studies have shown the potential of engineered muscle constructs (EMCs) to improve muscle reconstruction in vivo. EMCs composed of either muscle cells alone or in combination with endothelium and connective tissue, seeded on suitable scaffolds, have shown increased integration into the host upon implantation and myogenesis (*38*–*42*). Accordingly, we hypothesized that EMCs overexpressing GLUT4 would enhance glucose uptake and, concomitantly, will affect glucose homeostasis in diabetic animals. Thus, we constructed an EMC composed of skeletal muscle cells that were genetically modified to overexpress the GLUT4 transporter and implanted them into diabetic mice to then assess their glucose homeostasis.

RESULTS

Construction of WT-EMCs and their effect on glucose tolerance in DIO mice

To establish an implantation system in C57BL6 mice, we initially isolated skeletal muscle satellite cells (SCs) from the gastrocnemius

[1]Faculty of Biomedical Engineering, Technion—Israel Institute of Technology, Haifa, Israel. [2]Rina and Avner Schneur Center of Diabetes Research, Technion—Israel Institute of Technology, Haifa, Israel. [3]Rappaport Faculty of Medicine, Technion—Israel Institute of Technology, Haifa, Israel. [4]Program in Cell Biology, The Hospital for Sick Children, Toronto, Ontario, Canada. [5]Division of Endocrinology, Diabetes and Bone Diseases, Samuel Bronfman Department of Medicine, Ichan School of Medicine at Mount Sinai, New York, NY 10029, USA. [6]Department of Clinical Biochemistry and Pharmacology, Faculty of Health Sciences, Ben-Gurion University of the Negev, Beer-Sheva, Israel.
*Corresponding author. Email: shulamit@bm.technion.ac.il

muscle of C57BL6 mice and used them to create engineered tissue constructs to be implanted in diet-induced obesity (DIO) mice (Fig. 1A). The isolated cells, C57-WT (wild type), expressed PAX7, a transcription factor involved in the regulation of muscle precursor cell proliferation. The cells also expressed MyoD, a transcription factor indicating the activation and proliferation of the SC, and myogenin (MYOG), a transcription factor indicating their differentiation into myoblasts (Fig. 1B). To ensure myotube formation, C57-WT were seeded on two-dimensional (2D) plates and followed up to 10 days. The fusion of myoblasts was already noticed after 4 days, and defined, aligned, and multinucleated myotubes were observed on day 7 (fig. S1A). The expression of myogenic markers was assessed by using specific antibodies. The myotubes show distinctive myogenic morphology and express desmin, a muscle-specific intermediate filament; myosin heavy chain, a motor protein of thick muscle filaments; and MYOG (fig. S1B). These results confirm that the isolated SCs are able to proliferate and differentiate into mature myotubes.

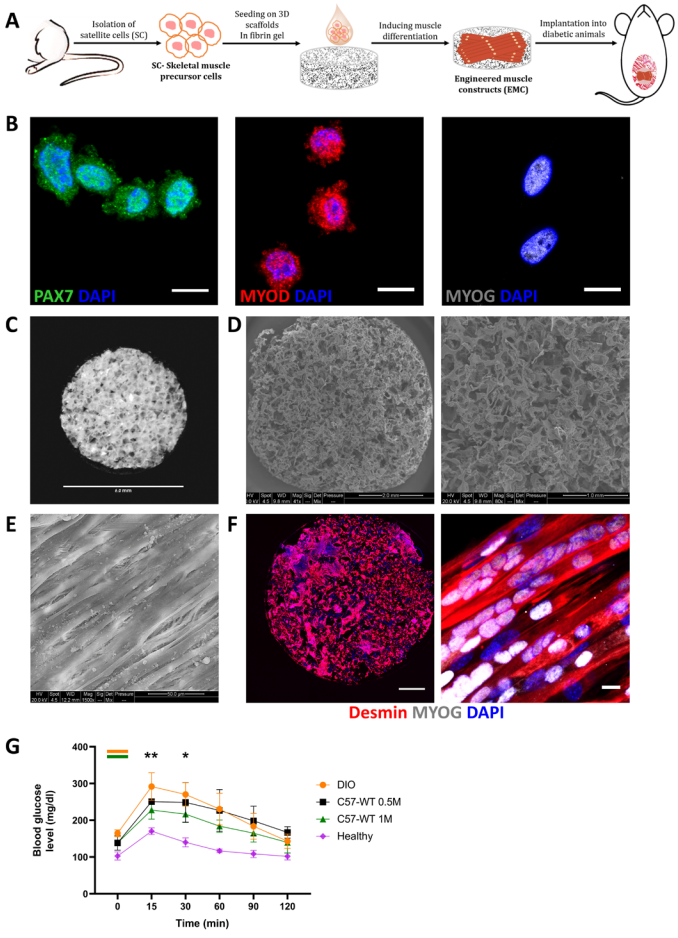

Fig. 1. Engineered wild-type (WT) muscle constructs. (**A**) Schematic presentation of experimental procedure. SCs are isolated from the hindlimb, and the cells are seeded in fibrin gel on 3D scaffolds. The seeded scaffolds are cultured in vitro to allow the formation of myotubes and afterward are implanted in the abdominal muscle of diabetic mice. (**B**) SC stained for PAX7 (green), MyoD (red), MYOG (gray), and cell nuclei in DAPI (blue). Scale bar, 10 μm. (**C**) PLLA/PLGA scaffold. Scale bar, 6 mm. (**D**) Scanning electron microscopy (SEM) images of PLLA/PLGA scaffold. Scale bars, 2 and 1 mm. (**E**) SEM images of engineered myotubes on the PLLA/PLGA scaffold after 3 weeks of in vitro culturing. Scale bar, 50 μm. (**F**) PLLA/PLGA scaffold seeded with 1×10^6 C57-WT cells per scaffold and cultured for 3 weeks in vitro and stained for desmin (red), MYOG (gray), and cell nuclei in DAPI (blue). Scale bars, 1000 and 10 μm. (**G**) GTT in DIO male mice, 1 week after implantation, implanted with constructs seeded with 0.5×10^6 ($n = 3$) and 1×10^6 ($n = 3$) C57-WT cells per scaffold, and cultured in vitro for 3 weeks, $^*P < 0.05$, $^{**}P < 0.01$.

EMCs were created by seeding the C57-WT on porous biodegradable poly-L-lactic acid (PLLA)/poly(lactic-coglycolic acid (PLGA) scaffolds (Fig. 1, C and D). The cells were cultured on the scaffolds for 3 weeks to allow the formation of defined and mature myotubes throughout the whole scaffold (Fig. 1, E and F). After ensuring the formation of muscle tissue, the EMCs were next implanted into DIO mice to see whether healthy WT cells would have any effect on the diabetic state. Mice were implanted in the abdominal muscle, with constructs seeded with 0.5×10^6 or 1×10^6 cells that were cultured for 3 weeks in vitro. The engineered construct constitutes up to 1.1% of the whole abdominal muscle weight and about 5% of the abdominal muscle surface area. To test the efficacy of the implants, we performed a glucose tolerance test (GTT) 1 week after the implantation. Mice implanted with the constructs that were seeded with the higher cell density showed significantly lower glucose levels at the 15-min point into the GTT (228 ± 14.5 mg/dl), compared to the same DIO mice before implantation (292 ± 13 mg/dl) (Fig. 1G). These results indicate that implantation of healthy C57-WT engineered muscle tissue can improve glucose tolerance in mice.

Effect of implantation of OEG4-EMCs in DIO mice

We then decided to test EMCs seeded with C57-WT cells that were transduced to overexpress the GLUT4 transporter (OEG4) (Fig. 2A). To establish stable overexpressing GLUT4 cells, C57-WT cells were transduced with pQCXIB retroviral plasmid. Quantitative polymerase chain reaction (qPCR) demonstrated 2.5-fold increase in GLUT4 mRNA expression compared to WT cells (Fig. 2B). Immunostaining of the transduced myotubes confirmed the significant overexpression of GLUT4 (Fig. 2, C and D). Next, the OEG4 cells were seeded on the scaffolds and cultured for 3 weeks in vitro. After the culturing period, the scaffolds were stained for desmin and MYOG to make sure that the genetic modification did not affect the myogenic characteristics and differentiation. The modified cells retain myogenic ability and form defined myotubes throughout the whole scaffold, such as the WT cells (Fig. 2E). There was no significant difference in the fiber (desmin) area and MYOG expression between the WT and the OEG4-EMCs (Fig. 2F). Next, to evaluate the glucose uptake ability of the EMCs in vitro, 2-deoxyglucose (2-DOG) uptake assay was performed. The constructs were incubated with a radioactive glucose analog, 3H-2-DOG, with and without insulin stimulation for 30 min. The C57-OEG4-EMCs presented significantly higher insulin-stimulated glucose uptake rate compared to their own basal uptake rate, a sevenfold increase. The C57-OEG4 also showed a fourfold higher insulin-stimulated glucose uptake rate compared to the C57-WT-EMCs (Fig. 2G).

To assess the in vivo efficacy of this genetic modification, C57-WT and OEG4 constructs were implanted in DIO mice that showed diabetic characteristics after 12 weeks on 60% high-fat diet (HFD) chow (fig. S2, A to D). The constructs were implanted in the abdominal muscle, where they fully integrated into the surrounding host tissue by 8 weeks after implantation (Fig. 3, A and C). After 16 weeks, the constructs were still visible in the tissue (Fig. 3, B and D). The constructs were found in close proximity to the host muscle,

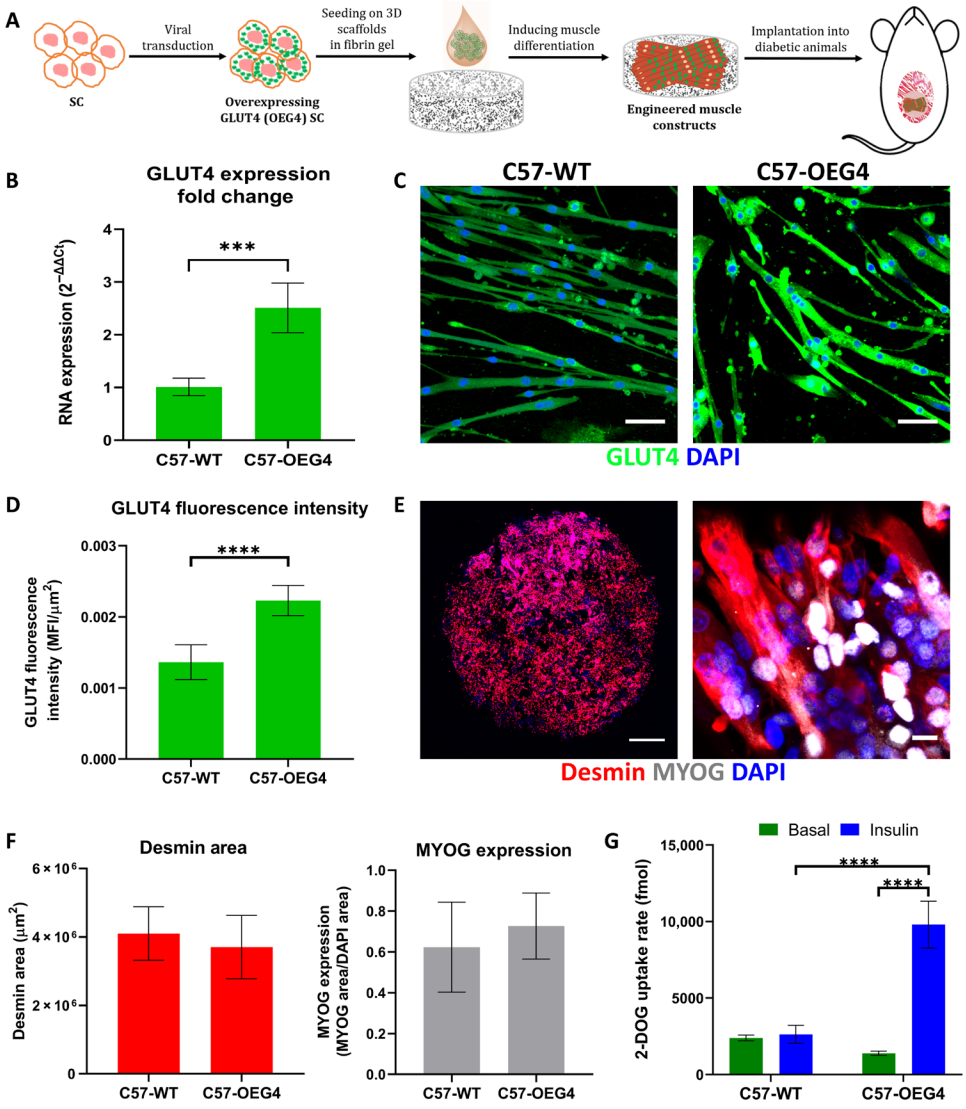

Fig. 2. Engineered OEG4 muscle constructs. (**A**) Schematic presentation of experimental procedure. SCs are transduced to overexpress the GLUT4 transporter. The OEG4 cells are seeded in fibrin gel on 3D scaffolds. The seeded scaffolds are cultured in vitro to allow the formation of myotubes and afterward are implanted in the abdominal muscle of diabetic mice. (**B**) qPCR analysis for the expression of GLUT4, normalized to the GAPDH housekeeping gene, ***$P < 0.001$. (**C**) C57 WT and OEG4 myotubes stained for GLUT4 transporter (green) and cell nuclei in DAPI (blue). Scale bar, 50 μm. (**D**) GLUT4 fluorescence intensity quantification, ****$P < 0.0001$. (**E**) PLLA/PLGA scaffolds seeded with 1×10^6 C57-OEG4 cells per scaffold, cultured for 3 weeks in vitro, and stained for desmin (red), MYOG (gray), and cell nuclei in DAPI (blue). Scale bars, 1000 and 10 μm. (**F**) Quantification of desmin area and MYOG expression of the engineered tissue formed on the PLLA/PLGA scaffolds. (**G**) 2-DOG uptake rates by WT and OEG4 constructs seeded with 1×10^6 cells per scaffold and cultured for 3 weeks in vitro, ****$P < 0.0001$.

and no scar tissue was observed. The constructs were retrieved after 16 weeks and stained for GLUT4 and desmin to visualize the engineered tissue (Fig. 3E). Viable myotubes were present in the construct, and 68 ± 5% of the total nuclei count were localized within the myotubes, similar to the host muscle in which 83.1 ± 8.6% of nuclei were localized in the myofibers (fig. S3). GLUT4 fluorescent signal was higher in OEG4-EMCs compared to WT-EMCs. RNA was extracted from the constructs and the surrounding muscle tissue, retrieved 16 weeks after implantation, and a qPCR was performed to validate the expression of GLUT4, which was higher in the OEG4-EMCs (Fig. 3F).

After implantation, fasting plasma glucose levels were followed up to 16 weeks. The glycemic values for each mouse were compared to the values before implantation. Mice implanted with OEG4-EMCs showed a reduction in fasting basal glucose levels, while mice that were implanted with WT-EMCs or underwent sham surgery maintained the same levels (Fig. 3, G and H). Initial plasma glucose levels of 190 ± 34 mg/dl dropped to 140 ± 18 mg/dl, a reduction of 26% for mice implanted with OEG4-EMCs (Fig. 3I).

To examine whether the implanted constructs had an effect on liver steatosis, a known complication of DIO model, the livers were extracted after 16 weeks and stained with oil red O (ORO) to visualize the lipid accumulation. Samples from mice implanted with OEG4-EMCs had a significantly lower lipid accumulation than mice implanted with WT-EMCs or those that underwent sham surgery (Fig. 3J). To test additional parameters of systemic effect,

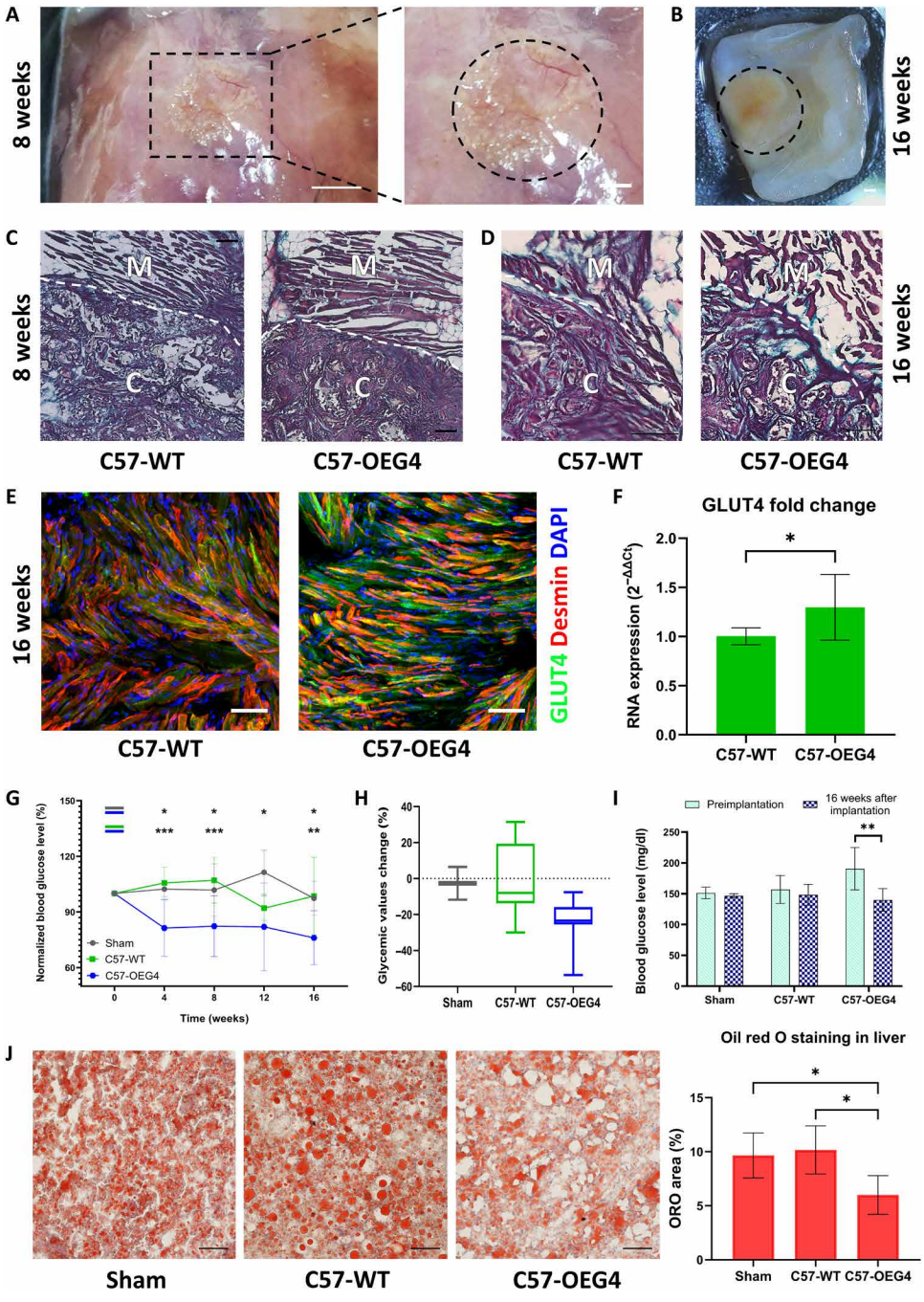

Fig. 3. Implantation of muscle constructs in DIO male mice. (**A**) Construct integration into the abdominal muscle of DIO mice 8 weeks after implantation. Scale bars, 5 and 2 mm. (**B**) Construct integration into the abdominal muscle of DIO mice 16 weeks after implantation. Scale bar, 0.5 mm. (**C**) Masson's trichrome histology staining of implanted constructs 8 weeks after implantation. Scale bar, 200 μm; dashed line indicates the connection site between the construct (marked with C) and the tissue (marked with M for muscle). (**D**) Masson's trichrome histology staining of implanted constructs 16 weeks after implantation. Scale bars, 200 μm; dashed line indicates the connection site between the construct (marked with C) and the tissue (marked with M for muscle). (**E**) C57 WT and OEG4 constructs retrieved after 16 weeks stained for GLUT4 transporter (green), desmin (red), and cell nuclei in DAPI (blue). Scale bars, 50 μm. (**F**) qPCR analysis of GLUT4 expression (normalized to the expression of the GAPDH housekeeping gene), in constructs and surrounding muscle tissue retrieved 16 weeks after implantation, $^{*}P < 0.05$. (**G**) Post-implantation follow-up of fasting basal blood glucose level in mice that had sham surgery ($n = 4$) and mice implanted with WT-EMCs ($n = 8$) and OEG4-EMCs ($n = 8$); values are normalized to the preimplantation values for each mouse, $^{*}P < 0.05$, $^{**}P < 0.01$, $^{***}P < 0.001$. (**H**) Change in glycemic values (%) for each mouse in all the groups at 16 weeks after implantation compared with the levels before implantation. (**I**) Fasting basal blood glucose levels before implantation and 16 weeks after implantation, $^{**}P < 0.01$. (**J**) Lipid ORO staining in liver samples from mice that had sham surgery ($n = 3$) and mice implanted with WT-EMCs ($n = 6$) and OEG4-EMCs ($n = 6$). Scale bars, 100 μm; quantification of the stained area, $^{*}P < 0.05$.

serum samples from healthy mice and the DIO mice (extracted 16 weeks after implantation) were ran in a chemical analyzer to measure levels of different analytes. Creatinine, sodium, chloride, and phosphate levels were the same between all groups, indicating proper renal function. Aspartate aminotransferase (AST), one of the liver health biomarkers, levels were significantly higher in mice implanted with WT-EMCs or those that underwent sham surgery, unlike OEG4-EMCs that showed lower levels that were not significantly different from the healthy mice. Bilirubin levels were also lower in mice implanted with OEG4-EMCs than in mice implanted with WT-EMCs or those that underwent sham surgery (fig. S4).

Transcriptome sequencing and proteome analysis of implanted constructs in DIO mice

To further explore the systemic effect, RNA sequencing (RNA-seq) and proteome analysis were performed on the samples of the retrieved constructs and the surrounding muscle tissue and on muscle tissue from healthy mice. A total of 54,446 genes were sequenced. Of the genes differentially expressed between DIO mice that underwent sham surgery and healthy controls (fig. S5A), a cluster of 91 genes showed similar expression between healthy mice and DIO mice implanted with EMCs (Fig. 4A). Gene interaction plot showed clusters of genes related to lipid and fatty acid metabolism (Fig. 4B and fig. S7A). Next, we looked into genes that were differentially expressed between the sham and OEG4 groups (fig. S5B). Further gene ontology analysis of these genes showed elevated expression of genes that regulate the production and secretion of interleukin-6 (IL-6), IL-10, and IL-13, which are muscle myokines that have a positive effect on metabolism (Fig. 4, C and D, and figs. S6A and S7B) and elevated expression of genes related to metabolic processes (Fig. 4, E and F, and figs. S6C and S7C). In addition, *IL-6ra*, *IL-10ra*, and *IL-13ra1* gene expression was elevated in OEG4-EMCs (fig. S6B).

Proteome was analyzed using mass spectrometry (MS), and a total of 1789 proteins were measured. Of the proteins differentially expressed between DIO mice that underwent sham surgery and healthy controls (fig. S8), a cluster of 44 proteins showed similar expression between healthy mice and DIO mice implanted with EMCs (Fig. 5A). Gene interaction plot showed clusters of lipid and fatty acid metabolism, similar to the RNA-seq, and muscle fiber development (Fig. 5B and fig. S9A). Next, we looked into proteins that were differentially expressed between the sham and OEG4 groups (Fig. 5C). Gene interaction plot showed clusters of metabolic process, respiratory burst, mitochondrial fission, and regulation of production and secretion of cytokines (Fig. 5D and fig. S9B).

Effect of implantation of OEG4-EMCs in Rag/MKR male mice

Rag/MKR, an immunodeficient mouse model for T2D, was also used to examine the beneficial effect of OEG4-engineered muscle in alleviating diabetes using nonautologous cells (L6 rat myoblasts), previously characterized by the Klip group for the OEG4 (*43*, *44*). We also confirmed the overexpression by immunostaining (fig. S10). The Rag/MKR mice are insulin resistant and allow the testing of the immediate effect of the implanted constructs. We initially characterized the myogenic abilities of the cells to create engineered muscle tissue. Cells were seeded on PLLA/PLGA scaffolds at the concentration of 0.5×10^6 cells per scaffold and cultured in vitro for 3 weeks. Defined myotubes can be noted throughout the whole scaffold (Fig. 6A), and similarly, there is no significant difference between the L6-WT and L6-OEG4-EMCs (Fig. 6B). Glucose uptake ability in vitro showed that the rate of insulin-stimulated uptake was significantly higher in L6-OEG4-EMCs compared to L6-WT-EMCs. L6-OEG4-EMCs also showed a twofold higher insulin-stimulated glucose uptake compared to C57-WT-EMCs and a twofold increase compared to their basal uptake rate (Fig. 6C).

Rag/MKR mice were implanted in the abdominal muscle with L6-WT, OEG4, and empty scaffolds, seeded with fibrin gel only. As with DIO mice, the constructs integrated fully into the surrounding host tissue 4 weeks after the implantation, as shown by histology (Fig. 7, A and B). Over a GTT, when challenged with a high dose of glucose (1 g/kg body weight), mice implanted with L6-OEG4-EMCs showed significantly lower blood glucose levels at 30 min (185 ± 39 mg/dl) compared to 247 ± 16 mg/dl for the L6-WT-EMCs and 294 ± 46 mg/dl for those implanted with empty constructs. In addition, glucose levels returned to basal values faster in L6-OEG4-EMC mice than in the control groups (Fig. 7C). L6-OEG4-EMC–implanted mice also had a significantly smaller area under curve (AUC) over the entire GTT than the empty and L6-WT-EMCs implanted mice (Fig. 7D), indicating improved glucose clearance. Using insulin tolerance test (ITT), mice with L6-OEG4-EMC implants showed a 62% reduction in plasma glucose levels compared to control mice, demonstrating improved insulin sensitivity (Fig. 7E).

DISCUSSION

Restoring metabolic activity of skeletal muscle is a promising and yet unexplored optional therapy for T2D. In this study, we have created a metabolically functional, engineered muscle tissue using muscle cells that overexpress the GLUT4 transporter. WT and OEG4 cells were seeded on polymeric biodegradable scaffolds and cultured up to 3 weeks; at this time point, the cells were fully differentiated, and the scaffold was covered with myotubes. The genetic modification did not affect the cell identity and myogenic abilities. Before implantation into diabetic animals, OEG4-EMCs showed a significantly higher glucose uptake rate compared with the WT-EMCs.

EMCs implanted in the abdominal muscle substituted only 1.1% of the total weight of the abdominal muscle and about 5% of the abdominal muscle surface area. The constructs integrated into the host muscle tissue and the mice implanted with the OEG4-EMCs showed significant improvement in glucose homeostasis and insulin sensitivity. DIO mice showed a reduction in fasting basal glucose levels for up to 4 months after implantation. Insulin-resistant mice showed improved tolerance to glucose overload and improved insulin sensitivity. DIO mice implanted with OEG4-EMCs also showed improved parameters related to nonalcoholic fatty liver disease, a known complication of obesity and metabolic syndrome, such as liver steatosis and AST serum levels.

The systemic effect demonstrated here corresponds with previous studies in TG mice overexpressing the GLUT4 transporter either in skeletal muscle alone or in both muscle and fat tissues. TG mice had higher glucose infusion rate under euglycemic hyperinsulinemic clamp and increased whole-body glucose disposal. In addition, they showed better glucose tolerance, higher insulin sensitivity, and lower fed and fasted glycemic values (*26*–*29*, *31*–*33*). We observed a similar systemic effect by replacing a small amount of skeletal muscle tissue, indicating that a moderate up-regulation over the endogenous gene is enough to influence glucose homeostasis. We assume that replacing only a partial fraction of GLUT4-expressing

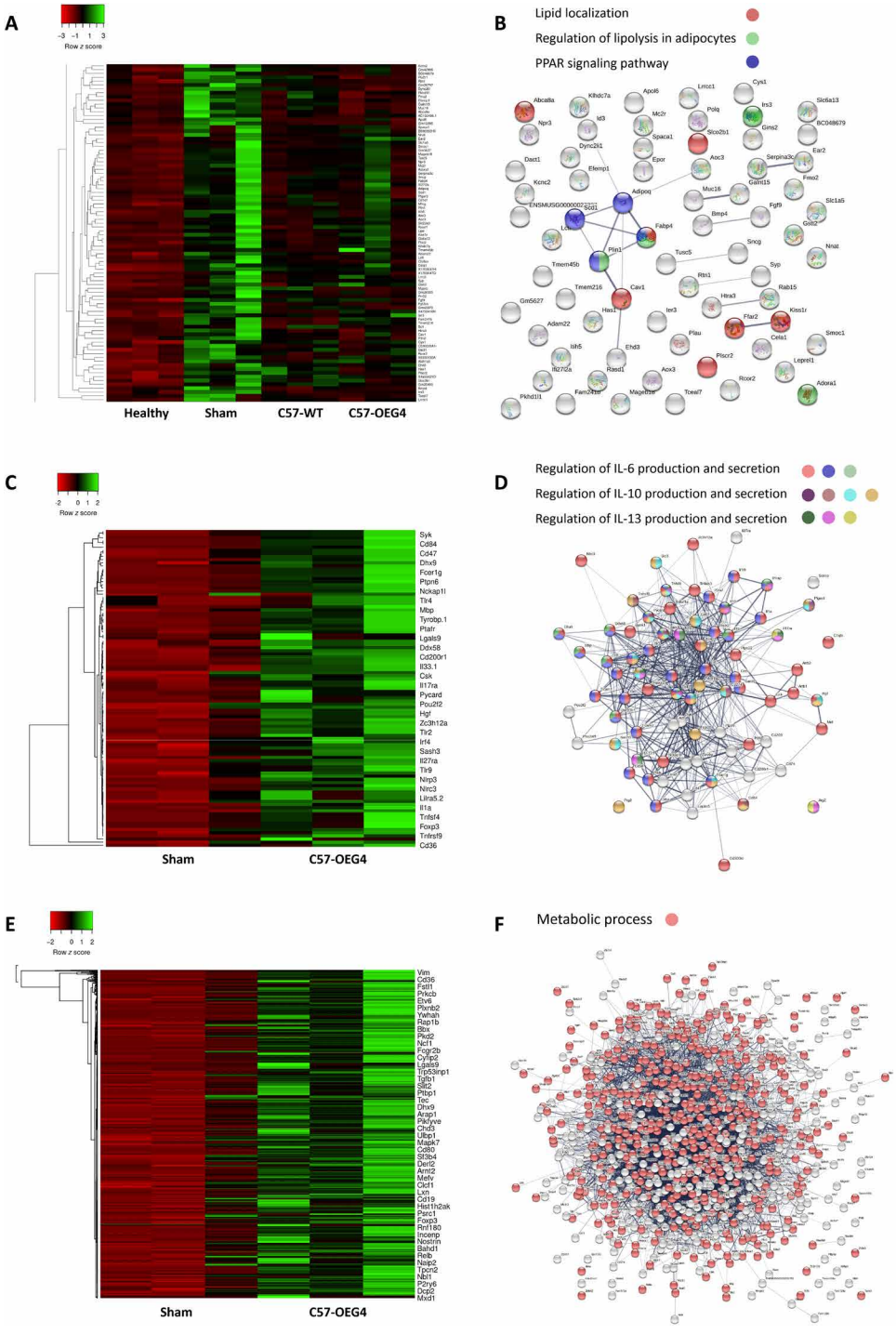

Fig. 4. RNA-seq analysis of implanted muscle constructs in DIO male mice. (**A**) Partial heatmap and (**B**) interaction plot of genes differentially expressed between healthy mice and DIO mice that underwent sham surgery, comparison between all mouse groups ($n = 3$ for each group). Genes related to lipid and fatty acid metabolism: lipid localization (light red), regulation of lipolysis in adipocytes (light green), and PPAR signaling pathway (blue). (**C**) Heatmap and (**D**) interaction plot of genes differentially expressed between mice implanted with OEG4-EMCs and mice that underwent sham surgery, which are related to the regulation of production (light red and blue) and secretion (light green) of IL-6, regulation of production (light blue and dark yellow) and secretion (purple and brown) of IL-10, and regulation of production (dark green and pink) and secretion (yellow) of IL-13. (**E**) Heatmap and (**F**) interaction plot of genes differentially expressed between mice implanted with OEG4-EMCs and mice that underwent sham surgery, which are related to metabolic processes (light red).

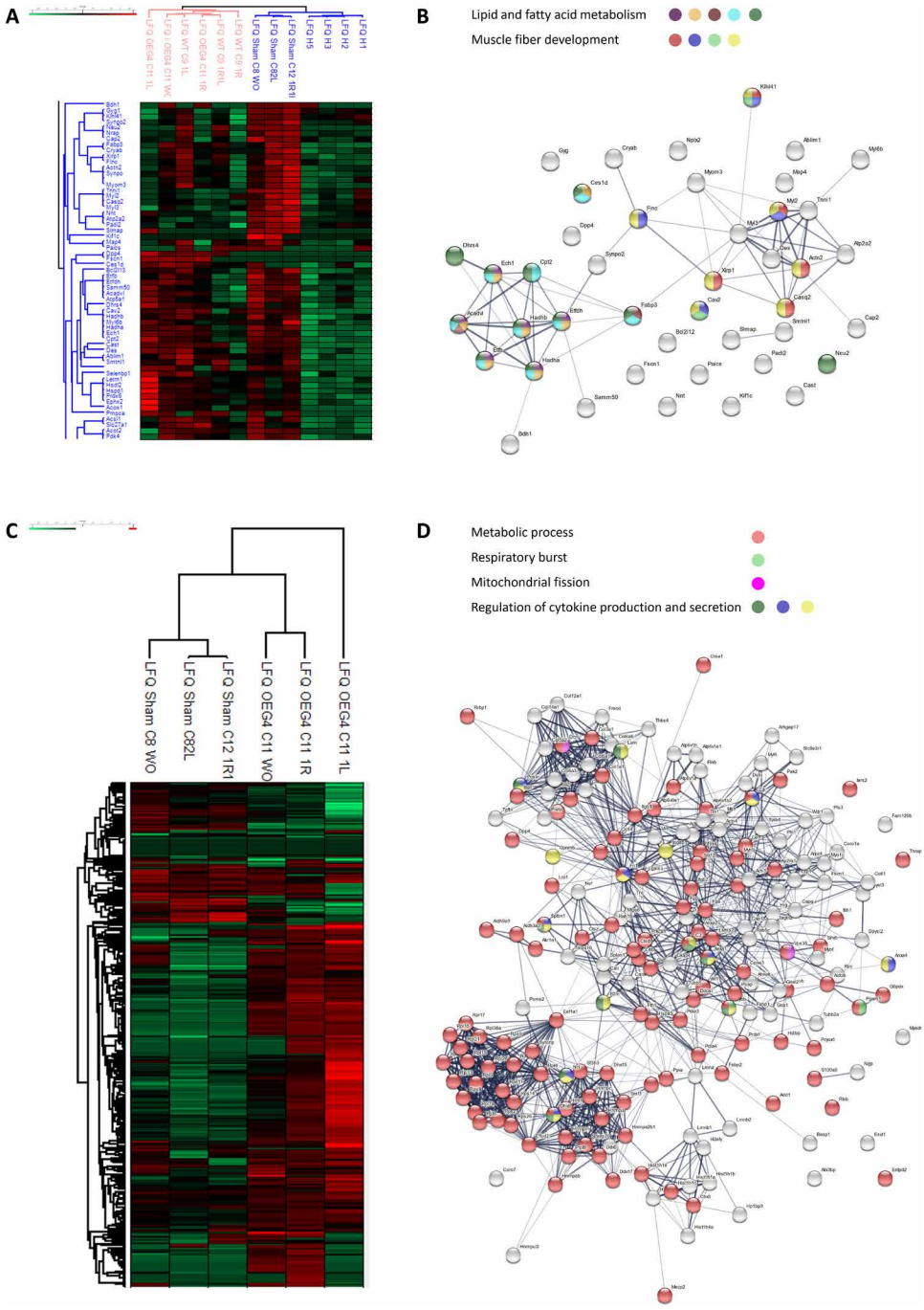

Fig. 5. Proteome analysis of implanted muscle constructs in DIO male mice. (**A**) Partial heatmap and (**B**) interaction plot of proteins differentially expressed in healthy mice versus DIO mice that underwent sham surgery, comparison between all mouse groups ($n = 4$ for healthy group and $n = 3$ for each of the other groups). Proteins related to lipid and fatty acid metabolism [fatty acid oxidation (dark purple and brown), fatty acid metabolism (dark yellow and light blue), and lipid metabolism (dark green)], and proteins related to muscle fiber development [myofibril assembly (light red) and muscle fiber and tissue development (blue, light green, and yellow)]. (**C**) Heatmap and (**D**) interaction plot of proteins differentially expressed between mice implanted with OEG4-EMCs and mice that underwent sham surgery. Proteins related to metabolic process (light red), respiratory burst (light green), mitochondrial fission (pink), and the regulation of production (dark green and yellow) and secretion of cytokines (blue).

tissue might avoid hypoglycemia presented in TG mice overexpressing GLUT4 (*26*).

The systemic effects could be attributed to the involvement of muscle-secreted myokines. Muscle secretome can influence skeletal muscle insulin resistance and T2D management. Skeletal muscle–secreted myokines have an autocrine, paracrine, and endocrine effect and can participate in metabolism regulation (*2*–*4*). For example, IL-15 is involved in glucose metabolic regulation, and its overexpression

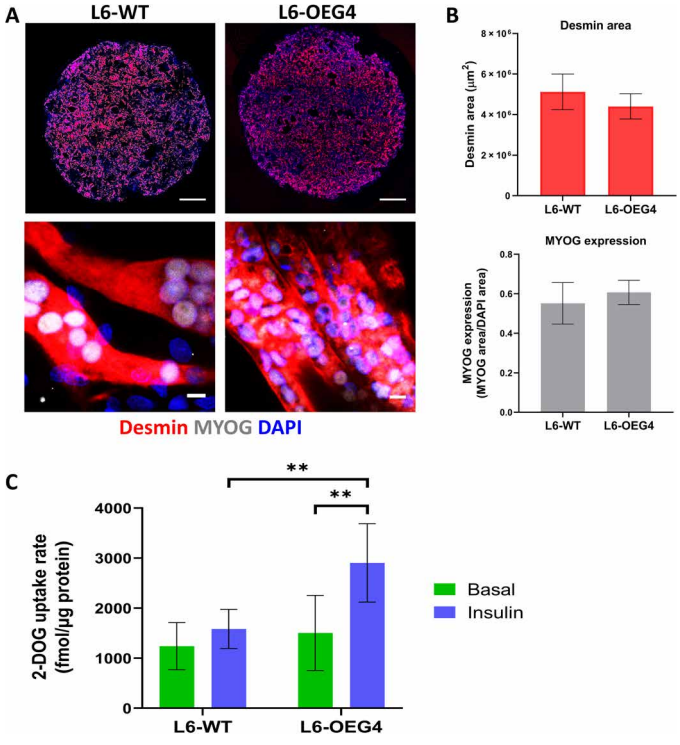

Fig. 6. L6 EMCs. (**A**) PLLA/PLGA scaffolds seeded with 0.5 × 10^6 L6-WT and L6-OEG4 cells per scaffold and cultured for 3 weeks in vitro, stained for desmin (red), MYOG (gray), and cell nuclei in DAPI (blue). Scale bars, 1000 and 10 μm. (**B**) Quantification of desmin area and MYOG expression of the engineered tissue formed on the PLLA/PLGA scaffolds. (**C**) 2-DOG uptake rates by L6-WT and L6-OEG4 constructs seeded with 0.5 × 10^6 cells per scaffold and cultured for 3 weeks in vitro, $^{**}P < 0.01$.

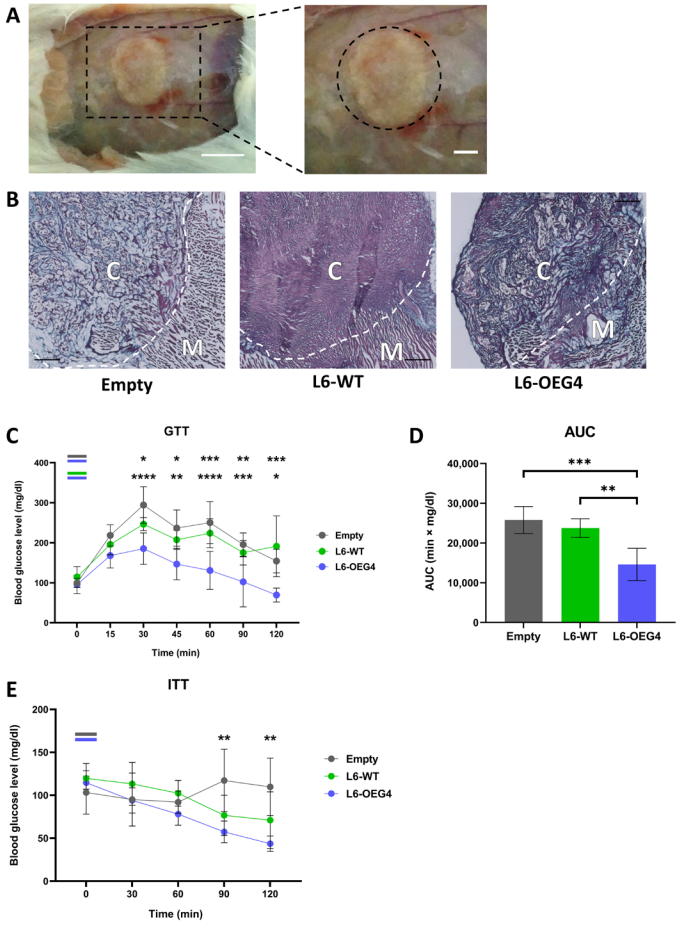

Fig. 7. Implantation of muscle constructs in Rag/MKR male mice. (**A**) Construct integration into the abdominal muscle of Rag/MKR mice 2 weeks after implantation, Scale bars, 5 and 2 mm. (**B**) Masson's trichrome histology staining of implanted constructs 4 weeks after implantation. Scale bars, 500 μm; dashed line indicates the connection site between the construct and the tissue. (**C**) GTT in Rag/MKR mice implanted with L6-WT ($n = 4$), L6-OEG4 ($n = 8$), and empty constructs ($n = 4$) 2 weeks after implantation, $^{*}P < 0.05$, $^{**}P < 0.01$, $^{***}P < 0.001$, $^{****}P < 0.0001$. (**D**) GTT corresponding AUC quantification, $^{**}P < 0.01$, $^{***}P < 0.001$. (**E**) ITT in Rag/MKR mice implanted with WT ($n = 3$), OEG4 ($n = 3$), and empty ($n = 4$) constructs 2 weeks after implantation, $^{**}P < 0.01$.

improves glucose tolerance (*45*). IL-15 also mediates the cross-talk between the muscle and adipose tissue and helps with reducing adipose tissue mass (*46*). IL-6 is involved in metabolic regulation, and it increases glucose uptake, insulin sensitivity, and fatty acid oxidation, without affecting white adipose tissue lipolysis. Furthermore, it has favorable effect on pancreatic β cells suppressing their apoptosis process (*46*–*48*). IL-10 contributes to increased insulin sensitivity and reduction of obesity-related inflammation (*49*, *50*); similarly, IL-13 reduces inflammatory response and insulin resistance (*51*, *52*).

Our data point to the possible role of genes regulating specific myokines and metabolic pathways in improving glucose homeostasis in general and specifically in our model. Transcriptome sequencing of samples of the retrieved constructs and the surrounding muscle tissue revealed elevated expression of genes that regulate the production and secretion of IL-6, IL-10, and IL-13 in samples retrieved from mice implanted with OEG4-EMCs. Mice implanted with OEG4-EMCs also showed elevation of genes and proteins related to metabolic processes and lipid metabolism.

This work demonstrates a unique approach for T2D management, which combines a long-term therapeutic effect with the advantages of autologous transplantation. New treatment options are mostly alternative long-term delivery systems for existing pharmaceutical agents to improve patient state and compliance (*14*–*16*). Using stimuli-responsive systems to treat diabetes is a promising direction. For example, Chen *et al.* (*17*) used a microneedle-array patch loaded with exendin-4 (glucagon-like peptide 1 analog) and mineral components as a stimuli-responsive delivery system. The mineral components aid in preserving the peptide and serve as a sensor to glucose stimuli, following which the exendin-4 will be released. Treated db/db mice showed lower basal glycemic values and a better tolerance reaction to glucose load. However, despite improving the delivery, these systems still introduce foreign materials to the body, which may lead to an immune response.

Since the diabetic profile varies greatly between patients, it is challenging to adjust a suitable general treatment that can provide glycemic normalization for many patients the same way (*53*). Our system uses internal resources of the organism by introducing genetic modification to the autologous muscular tissue. The EMCs integrate into the host muscle and respond to the internal signaling, governing glucose homeostasis and providing an improved precision (personalized) medicine approach.

The platform presented in this study provided long-lasting overexpression of the GLUT4 transporter and showed a favorable effect on glucose homeostasis in diabetic mice. However, further research is needed to assess additional physiological parameters that may have been affected by the implanted constructs. DIO is one of the main models to investigate T2D, but it does not represent the human pathogenesis fully, so alternative animal models that mimic the human condition better are needed, as well as other ways to modify the expression of GLUT4 to avoid viral transduction.

The EMC may serve as a general platform for the constitutive expression of other proteins. It can be used as a therapeutic tool for enzymatic deficiency disorders, for which the treatment is mostly lifestyle modulation for supportive therapy and intravenous delivery of the down-regulated or missing enzymes (*54*–*56*).

In summary, we showed a long-term effect of glucose homeostasis normalization for diabetic mice, following implantation of an engineered muscle tissue constructs. This effect suggests the use of genetically modified EMCs as a novel therapeutic modality for T2D.

MATERIALS AND METHODS

Cell isolation and cell culture

Primary mouse SCs were isolated from the gastrocnemius muscle of 8-week-old male C57BL6 mice. The muscle was separated from the surrounding connective tissue, and the adjacent bone and tendons were dissected and minced. The muscle segments were placed under agitation for 1 hour at 37°C in 0.25% trypsin-EDTA solution (Biological Industries) for enzymatic dissociation and later filtered through a 100-μm membrane cell strainer (BD Falcon). The filtrate was centrifuged twice at room temperature (RT) for 10 min at 1200*g*, and the pellet was resuspended with a rich proliferation medium, BIO-[human amniotic fluid (AMF)]-2 medium (Biological Industries). Myogenic cells were separated from fibroblasts using a plating technique based on their adherence to gelatin-coated surfaces. To induce differentiation of myoblasts into myotubes, the SCs were cultured in Dulbecco's Modified Eagle Medium (Gibco), supplemented with 5% Horse serum (HS) (Biological Industries), 1% Pen-Strep (PS) (Biological Industries), and 1% GlutaMAX (Gibco).

L6 myoblasts were cultured in MEM-α medium (Biological Industries) supplemented with 10% fetal bovine serum (FBS) (HyClone, Thermo Fisher Sceintific), 1% PS (Biological Industries), and 0.1% amphotericin B (Biological Industries). L6-GLUT4myc (overexpressing GLUT4) cells were added directly in the culture plate with blasticidin HCl (2 μg/ml; Calbiochem) antibiotic for positive selection of OEG4 cells. To induce differentiation of myoblasts into myotubes, FBS levels were reduced to 2%. All cells were incubated in a 5% CO_2 humidified atmosphere at 37°C.

2D immunofluorescence

Cells were washed with phosphate-buffered saline (PBS) 1× (Gibco) and then fixed in 4% paraformaldehyde (PFA) (ChemCruz, Santa Cruz Biotechnology) for 10 min at RT. The fixation solution was removed, and the cells were washed with PBS 1×. Next, the cells were treated with 0.1% Triton X-100 (Bio-Lab Ltd.) for 10 min at RT to permeabilize the cells. The permeabilization solution was removed, and cells were washed with PBS 1×. Then, the cells were incubated overnight (ON) at 4°C, with the primary antibodies (antibodies details are enclosed in table S1) diluted with the blocking solution of 5% bovine serum albumin (BSA) (Millipore) in PBS. The following day, the cells were washed with PBS 1× and then incubated for 1 hour at RT, with the secondary antibodies and 4′,6-diamidino-2-phenylindole (DAPI) (Sigma-Aldrich) diluted in PBS 1×. Then, they were washed with PBS 1× and stored in it until imaging. The cells were imaged using a confocal microscope (LSM700, Ziess). Fiji software (ImageJ) was used to process and analyze the images.

Scaffold generation

Salt leaching technique was used to create porous biodegradable scaffolds out of PLLA (Polysciences, Warrington) and PLGA (Boehringer Ingelheim). The constructs have a pore size of 212 to 600 μm and 93% porosity (*57*, *58*). From each polymer, a 5% (w/v) solution was prepared separately by dissolving 0.5 g of polymer in 10 ml of chloroform (Bio-Lab Ltd). The polymers were mixed in a 1:1 ratio to create a PLLA/PLGA solution. NaCl (0.4 g) was dissolved in 0.24 ml of PLLA/PLGA solution in Teflon cylinder molds (18 mm internal diameter). The Teflon molds were left ON to allow for chloroform evaporation, after which, the scaffolds were gently removed from the molds and placed into histology cassettes. The salt was leached by washing with distilled water on a magnetic stirring plate; the water was exchanged every hour for 6 to 8 hours. The scaffolds were dried and frozen ON at −80°C. The following day, the scaffolds were lyophilized ON and kept dry under vacuum until use. One day before seeding, round pieces of scaffold material of 6-mm diameter were prepared using a biopsy punch (Miltex). These pieces were sterilized in 70% ethanol ON. Before seeding, the scaffolds were washed twice in PBS 1× (Sigma-Aldrich) and dried using vacuum.

Engineered 3D tissue construction

Muscle cells were cultured up to 70% confluency and then washed with PBS 1× and trypsinized with 2× Trypsin-EDTA (Biological Industries), centrifuged at RT at 200*g* for 4 min, and resuspended in 6 μl of a 1:1 mixture of fibrinogen (15 mg/ml) (Sigma-Aldrich) and thrombin (20 U/ml) (Sigma-Aldrich). The cell suspension, 0.5×10^6 to 1×10^6 cells per scaffold, was seeded into PLLA/PLGA scaffolds and allowed to dry for 30 min at 37°C and 5% CO_2. After solidification, 2 ml of growth medium was added to each well. After 2 days, the scaffolds were transferred to a new plate using sterile forceps, and 2 ml of differentiation medium was added to each well.

Scanning electron microscopy imaging

PLLA/PLGA scaffolds with and without cells were scanned in the Quanta 200 microscope (FEI). Cell-seeded scaffolds were fixed in 2.5% glutaraldehyde in 0.1 M cacodylate (Sigma-Aldrich) for 5 min and dehydrated with increasing ethanol (GADOT-GROUP) gradient of 70, 85, 95, and 100% for 5 min each. The scaffolds were then soaked in hexametyldisilazane (Sigma-Aldrich) for 5 min and, afterward, were left to air dry ON at RT. Before the scanning, all the samples were coated with a gold-palladium mixture.

Immunofluorescent whole mount staining

Scaffolds seeded with cells were cultured for 3 weeks in vitro. Whole scaffolds were washed with PBS 1× solution and then fixed in 4% PFA for 10 min, the fixation solution was removed, and the scaffolds were washed with PBS 1×. Next, the scaffolds were treated with 0.3% Triton X-100 for 10 min. Then, the scaffolds were washed with PBS and soaked in blocking solution (5% BSA) for 2 hours at RT or ON at 4°C. The following day, samples were incubated ON

at 4°C with a solution of primary antibodies diluted in blocking solution. Last, scaffolds were washed with PBS 1× and incubated with secondary antibodies and DAPI solution diluted in PBS 1× for 2 hours at RT. Next, scaffolds were washed with PBS 1× and stored in it until imaging. The images of the engineered constructs were taken using a confocal microscope (LSM700, Ziess). Fiji software was used to process and analyze the images.

GLUT4 retroviral transduction

C57-SC were transduced with the pQCXIB retroviral plasmid containing the GLUT4 cDNA (*59*, *60*) using the Retro-X universal packaging system (Takara Bio, USA). SCs were seeded at a concentration of 25,000 cells per well in a 24-well plate; the following day, they were incubated with the viral particles for 24 hours. The transduction was either in the presence of polybrene (2 to 6 μg/ml) (Sigma-Aldrich) or on plates coated with RetroNectin (20 to 75 μg/ml) (Takara Bio, USA). The transduction medium was replaced after 24 hours, and the cells were incubated for 48 hours to allow expansion. Stable expressing cells were positively selected using blasticidin HCl antibiotic (10 μg/ml).

RNA extraction from cells

RNA was extracted from C57 WT and OEG4 cells using the RNeasy extraction kit (Qiagen) according to the manufacturer's instructions. RNA concentration was measured with a NanoDrop (NanoDrop One, Thermo Fisher Scientific). cDNA was synthetized using the high-capacity cDNA Reverse Transcription Kit (Applied Biosystems, Thermo Fisher Scientific) according to the manufacturer's instructions. cDNA was kept at 4°C up to 4 weeks.

Quantitative polymerase chain reaction

qPCR was performed using the TaqMan Fast Advanced Master Mix (Applied Biosystems, Thermo Fisher Scientific) according to the manufacturer's instructions. The TaqMan Gene Expression Assay (Thermo Fisher Scientific) primers were used for GLUT4 (Mm00436615_m1) and glyceraldehyde-3-phosphate dehydrogenase (GAPDH) (Mm99999915_g1). The reaction was performed in the QuantStudio1 (Applied Biosystems, Thermo Fisher Scientific). The results are presented as $2^{-\Delta\Delta ct}$ and normalized to the GAPDH housekeeping gene.

2-DOG uptake in the EMCs

The method was adapted from Armoni *et al.* (*61*). Cells were seeded on PLLA/PLGA scaffolds at a seeding concentration of 0.5×10^6 or 1×10^6 cells per scaffold in a 12-well plate and cultured 3 weeks in vitro. After 3 weeks, the constructs were washed with PBS 1× and then were serum-starved for 3 hours followed by 30 min incubation in either absence or presence of 100 nM insulin (basal and insulin, respectively) (NovoRapid, Novo Nordisk). 2-DOG (0.1 mM; 2 μCi) (PerkinElmer) was then added for an additional 20 min. The uptake was terminated by three rapid washes in ice-cold Krebs Ringer Phosphate (KRP) buffer. Following the last wash, the scaffolds were minced manually with scissors, vortexed, and transferred into 500 μl of 1% SDS in 1 N NaOH solution at 80°C for 1 hour; then, 50 μl of the samples was taken to measure cellular protein levels by bicinchoninic acid (BCA) protein assay. The rest was added to 4 ml of scintillation fluid (Ultima Gold) in glass vials. 2-DOG–associated radioactivity was counted using a beta-counter (Tri-Carb 2100 TR and Tri-Carb 2810 TR, PerkinElmer).

BCA assay

Protein levels for each sample were determined using a BCA kit (Thermo Fisher Sceintific). The samples were treated with the kit reagents in a 96-well plate according to the manufacturer's instructions. The plate was incubated in 37°C for 30 min and cooled at RT for 10 min. Afterward, the optical density was read at a wavelength of 562 using a plate reader (800 TS microplate reader, Biotek).

DIO animal model

All the animal procedures were performed according to protocols approved by the Institutional Animal Care and Use Committee of the Technion Israel Institute of Technology. C57BL6 male mice at the age of 7 to 8 weeks were monitored for 2 to 3 weeks for basal weight and glucose levels. Mice were fasted for 6 hours, and glucose level was determined using a glucometer (Freedom Lite, FreeStyle). After establishing basal levels, the mice were transferred from regular chow to HFD chow (Teklad) with 60% of fat content. Fasting glucose blood levels and weight were followed up during the 12 weeks of diabetes induction.

Rag/MKR mice model

The $Rag1^{-/-}$/MKR mice are an immunodeficient mouse model crossed to the insulin-resistant mice that demonstrate overt diabetes in the male mice and hyperinsulinemia/insulin resistance in the female mice (*62*).

Intramuscular implantation in the abdominal muscle

The engineered constructs were implanted after an in vitro culturing period of 2 to 3 weeks. Mice were anesthetized using ketamine-xylazine cocktail (100 and 10 mg/kg body weight, respectively; ketamine was from Vetoquinol and xylazine was from EuroVet), delivered using a 27-gauge needle via an intraperitoneal injection or with 2.5% isoflurane (Abbott). A portion of the fur of the animal was removed by shaving and depilation cream, at the abdomen. A small incision was made allowing access to the linea-alba and surrounding tissue, where a 2- to 3-mm wound was created by removing a full thickness tissue section from the abdominal muscle. The constructs were sutured into the defect margins with 8-0 silk sutures (Assut Sutures). Outer skin was closed and sutured using 5-0 AssuCryl surgical sutures (Assut Sutures). Mice were monitored closely for 2 hours to ensure full recovery.

Glucose tolerance test

Blood glucose levels were measured using a glucometer (FreeStyle, Abbot). After a 6-hour fast, the animals were injected intraperitoneally with a 10% w/v glucose solution (B Braun). Blood samples were obtained at 0, 15, 30, 45, 60, 75, 90, and 120 min following glucose administration.

Insulin tolerance test

Blood glucose levels were measured using a glucometer (FreeStyle, Abbot). After a 6-hour fast, the animals were injected intraperitoneally with insulin (1 U/kg body weight) (Novorapid, NovoNordisk). Blood samples were obtained at 0, 30, 60, 90, and 120 min following glucose administration.

Masson's trichrome histological stain

The constructs and surrounding muscle tissue were retrieved between 2 and 16 weeks after implantation. The samples were washed

with PBS 1× and fixed with 4% PFA for 20 min, the fixation solution was removed, and the samples were washed with PBS 1×. Afterward, the samples were incubated ON in 30% sucrose solution at 4°C and then embedded in optimal cutting temperature compound (OCT) (Tissue-Tek) for cryosectioning. For a Masson's trichrome staining, the samples were cut into 5-μm-thick sections. The slides were initially air-dried and stained with Mayer's hematoxylin (Sigma-Aldrich) for 5 min, followed by washes with distilled water and trichrome staining (Sigma-Aldrich) for 2 min. Next, the slides were washed twice with 0.2% glacial acetic acid and with double-distilled water. Afterward, the slides were dehydrated by serial immersions in increasing gradient of ethanol and finally dipped in xylene and covered with EUKITT mounting (Sigma-Aldrich). The slides were imaged with the Axio Observer 7 microscope (Ziess). Images were processed using the Zen Blue software (Ziess).

Immunofluorescence in cryosections

Slides with cryosections with a thickness of 10 μm were washed with PBS 1× and incubated with 0.5% Tween-20 (Sigma-Aldrich) for 20 min and then washed with PBS 1×. Next, the slides were incubated in blocking solution (5% BSA) for 1 hour. Then, the slides were incubated ON at 4°C, with a solution of primary antibodies diluted in blocking solution. The following day, the slides were washed with PBS 1× and incubated with secondary antibodies and DAPI solution diluted in PBS 1× for 1 hour at RT and later washed with PBS 1×. Next, the slides were mounted with Fluoromount-G (SouthernBiotech) and covered with coverslips. The images of sections were taken using a confocal microscope (LSM700, Ziess). Fiji software and IMARIS software (Bitplane Inc.) were used to process and analyze the images.

Blood biochemical assay

Blood was collected from mice into Lavender BD Microtainer collection tubes (Thermo Fisher Scientific). Serum was separated by centrifugation for 10 min at 1600*g* at 4°C and kept at −80°C. The biochemical levels of different components were measured in Cobas 6000c501 analyzer (Roche).

ORO staining in liver samples

The livers were retrieved 16 weeks after implantation and washed with PBS 1×. Then, the samples were fixed with 4% PFA for 20 min, the fixation solution was removed, and the samples were washed with PBS 1×. Afterward, the samples were incubated ON in 30% sucrose solution at 4°C and then embedded in OCT compound (Tissue-Tek) for cryosection. For ORO staining, the samples were cut into 10-μm-thick sections. The slides were dipped in 60% isopropanol and stained with a working solution of ORO (Sigma-Aldrich) in isopropanol (3:2) for 15 min. Then, the slides were washed with distilled water and stained with hematoxylin (Sigma-Aldrich) for 2 min. Next, the slides were washed with tap and distilled water and mounted with Fluoromount-G and covered with coverslips. For histopathological evaluation by a veterinary pathologist, the slides were sent to PATHO-LOGICA Ltd. The ORO-stained area was evaluated by a scoring scale. The slides were imaged with the Axio Observer 7 microscope (Ziess). Images were processed using the Zen Blue software (Ziess).

RNA extraction from tissue

The constructs and surrounding muscle tissue were retrieved 16 weeks after implantation and kept in RNAlater (Qiagen) at −80°C. On the day of extraction, the samples were thawed on ice and washed with cold PBS 1×. RNA was extracted with TRI reagent (Sigma-Aldrich) according to the manufacturer's instructions. RNA concentration was measured with a Qubit 4 Fluorometer (Thermo Fisher Scientific). cDNA was synthetized using the high-capacity cDNA Reverse Transcription Kit, according to the manufacturer's instructions. cDNA was kept at 4°C up to 4 weeks.

RNA sequencing

Twelve RNA libraries were generated using SMARTer Stranded Total RNA-Seq Kit v2 Pico Input Mammalians Prep Kit (Takara) according to the manufacturer's instructions and sequenced on Illumina NextSeq550, 75 single-end runs. The number of reads ranged from 35,944,877 to 48,164,957 per sample. The reads were mapped to the mouse genome (*GRCm38*) using Tophat2 version 2.1.0 (*63*) with up to three mismatches allowed per read, and the minimum and maximum intron sizes were set to 50 and 100,000, respectively; an annotation file was provided to the mapper. The percentage of uniquely mapped reads ranged from 67.4 to 77.3 per sample. Only uniquely mapped reads were counted to genes using "HTSeq-count" package version 0.11.2 with "union" mode (*64*). Normalization and differential expression analyses were conducted using DESeq2 R package version 1.28.1 (*65*). Sample preparation, sequencing, quality control, and initial bioinformatic analyses were conducted by the "Technion Genome Center" Life Science and Engineering Interdisciplinary Research Center, Technion, Haifa, Israel. Heatmaps were generated using the Heatmapper tool (*66*). Gene ontology analysis was done with GOrilla tool (*67*, *68*). Gene interaction plots were generated using the STRING database (*69*).

Proteome analysis

The constructs and surrounding muscle tissue were retrieved 16 weeks after implantation. Samples were sent to Technion's Smoler Proteomics Center, where they were extracted in 8 M Urea and 100 mM ammonium bicarbonate (ABC) and sonicated. Laemmli sample buffer was added, and the proteins were separated on SDS–polyacrylamide gel electrophoresis followed by Coomassie staining and destaining. Each lane was sliced into two fractions, and the proteins in the gel were reduced with 3 mM dithiothreitol in 100 mM ABC (60°C for 30 min), modified with 10 mM iodoacetamide in 100 mM ABC (in the dark at RT for 30 min), and digested in 10% acetonitrile and 10 mM ABC with modified trypsin (Promega) at a 1:10 enzyme-to-substrate ratio ON at 37°C. The tryptic peptides were desalted using C18 tips (Top tip, Glygen), dried, and resuspended in 0.1% formic acid.

The peptides were resolved by reversed-phase chromatography on 0.075 × 200 mm fused silica capillaries (J&W) packed with Reprosil reversed-phase material (Dr. Maisch GmbH). The peptides were eluted with linear 120 min gradient of 5 to 28%, 15 min gradient of 28 to 95%, and 25 min at 95% acetonitrile with 0.1% formic acid in water at flow rates of 0.15 μl/min. MS was performed using a Q Exactive HF mass spectrometer (Thermo Fisher Scientific) in a positive mode using repetitively full MS scan followed by collision-induced dissociation higher-energy C-trap dissociation (HCD) is a CID (collision induced dissociation) technique of the 20 most dominant ions selected from the first MS scan. The MS data were analyzed using the MaxQuant software 1.5.2.8 (*70*) for peak picking and identification using the Andromeda search engine versus the mouse proteome from the UniProt database with 1% false discovery rate with a mass tolerance of 6 ppm. Oxidation on methionine and

acetylation on the N terminus were accepted as variable modifications, and carbamidomethyl on cysteine was accepted as static modifications. Minimal peptide length was set to seven amino acids, and a maximum of two miscleavages was allowed. The data were quantified by label-free analysis using the same software based on extracted ion currents of peptides. Statistical analysis of the identification and quantization results was done using Perseus 1.6.10.43 software (*71*). A *t* test was performed on the normalized intensities (label-free quantification). Proteins with $P < 0.05$ were defined as differentially expressed. Differentially expressed proteins with a $\log_2$ (fold change) higher than 0.8 or lower than −0.8 were defined as having increased or decreased expression, respectively. Gene interaction plots were generated using the STRING database (ELIXIR).

Statistical analysis

Data are presented as means ± SD. Data were analyzed using a computerized statistical program, GraphPad Software. The applied statistical tests that were used to determine group differences are an unpaired Student's *t* test for GLUT4 overexpression, engineered tissue properties and DIO follow-up at the end point, an ordinary one-way analysis of variance (ANOVA) for ORO-stained area in liver samples, chemical analyte panel, and AUC of GTT assay. Two-way ANOVA was performed for 2DOG uptake rates, GTT and ITT assays, and normalization of glycemic value follow-up in DIO mice. *P* value below 0.05 was taken to indicate a statistically significant difference.

SUPPLEMENTARY MATERIALS

Supplementary material for this article is available at https://science.org/doi/10.1126/sciadv.abg3947

View/request a protocol for this paper from *Bio-protocol*.

REFERENCES AND NOTES

1. W. R. Frontera, J. Ochala, Skeletal muscle: A brief review of structure and function. *Calcif. Tissue Int.* **96**, 183–195 (2015).
2. B. K. Pedersen, M. A. Febbraio, Muscles, exercise and obesity: Skeletal muscle as a secretory organ. *Nat. Rev. Endocrinol.* **8**, 457–465 (2012).
3. J. Giudice, J. M. Taylor, Muscle as a paracrine and endocrine organ. *Curr. Opin. Pharmacol.* **34**, 49–55 (2017).
4. M. C. K. Severinsen, B. K. Pedersen, Muscle–organ crosstalk: The emerging roles of myokines. *Endocr. Rev.* **41**, 594–609 (2020).
5. R. A. DeFronzo, D. Tripathy, Skeletal muscle insulin resistance is the primary defect in type 2 diabetes. *Diabetes Care* **32** (Suppl. 2), S157–S163 (2009).
6. E. J. Gallagher, D. Leroith, E. Karnieli, Insulin resistance in obesity as the underlying cause for the metabolic syndrome. *Mt. Sinai J. Med.* **77**, 511–523 (2010).
7. S. E. Kahn, M. E. Cooper, S. Del Prato, Pathophysiology and treatment of type 2 diabetes: Perspectives on the past, present, and future. *Lancet* **383**, 1068–1083 (2014).
8. F. Ismail-Beigi, Pathogenesis and glycemic management of type 2 diabetes mellitus: A physiological approach. *Arch. Iran. Med.* **15**, 239–246 (2012).
9. E. W. Gregg, N. Sattar, M. K. Ali, The changing face of diabetes complications. *Lancet Diabetes Endocrinol.* **4**, 537–547 (2016).
10. W. C. Knowler, E. Barrett-Connor, S. E. Fowler, R. F. Hamman, J. M. Lachin, E. A. Walker, D. M. Nathan; Diabetes Prevention Program Research Group, Reduction in the incidence of type 2 diabetes with lifestyle intervention or metformin. *N. Engl. J. Med.* **346**, 393–403 (2002).
11. L. Lipscombe, G. Booth, S. Butalia, K. Dasgupta, D. T. Eurich, R. Goldenberg, N. Khan, L. MacCallum, B. R. Shah, S. Simpson, Pharmacologic glycemic management of type 2 diabetes in adults. *Can. J. Diabetes* **42**, S88–S103 (2018).
12. H. E. Resnick, G. L. Foster, J. Bardsley, R. E. Ratner, Achievement of American Diabetes Association clinical practice recommendations among U.S. adults with diabetes, 1999-2002: The National Health and Nutrition Examination Survey. *Diabetes Care* **29**, 531–537 (2006).
13. E. H. B. Lin, W. Katon, M. Von Korff, C. Rutter, G. E. Simon, M. Oliver, P. Ciechanowski, E. J. Ludman, T. Bush, B. Young, Relationship of depression and diabetes self-care, medication adherence, and preventive care. *Diabetes Care* **27**, 2154–2160 (2004).
14. O. Veiseh, B. C. Tang, K. A. Whitehead, D. G. Anderson, R. Langer, Managing diabetes with nanomedicine: Challenges and opportunities. *Nat. Rev. Drug Discov.* **14**, 45–57 (2014).
15. J. Yu, Y. Zhang, H. Bomba, Z. Gu, Stimuli-responsive delivery of therapeutics for diabetes treatment. *Bioeng. Transl. Med.* **1**, 323–337 (2016).
16. Y. Xu, M. Van Hul, F. Suriano, V. Préat, P. D. Cani, A. Beloqui, Novel strategy for oral peptide delivery in incretin-based diabetes treatment. *Gut* **69**, 911–919 (2020).
17. W. Chen, R. Tian, C. Xu, B. C. Yung, G. Wang, Y. Liu, Q. Ni, F. Zhang, Z. Zhou, J. Wang, G. Niu, Y. Ma, L. Fu, X. Chen, Microneedle-array patches loaded with dual mineralized protein/peptide particles for type 2 diabetes therapy. *Nat. Commun.* **8**, 1777 (2017).
18. J. Boucher, A. Kleinridders, C. Ronald Kahn, Insulin receptor signaling in normal and insulin-resistant states. *Cold Spring Harb. Perspect. Biol.* **6**, a009191 (2014).
19. S. Huang, M. P. Czech, The GLUT4 glucose transporter. *Cell Metab.* **5**, 237–252 (2007).
20. A. Klip, T. E. McGraw, D. E. James, Thirty sweet years of GLUT4. *J. Biol. Chem.* **294**, 11369–11381 (2019).
21. R. J. Sargeant, M. R. Paquet, Effect of insulin on the rates of synthesis and degradation of GLUT1 and GLUT4 glucose transporters in 3T3-L1 adipocytes. *Biochem. J.* **290**, 913–919 (1993).
22. M. A. Herman, B. B. Kahn, Glucose transport and sensing in the maintenance of glucose homeostasis and metabolic harmony. *J. Clin. Invest.* **116**, 1767–1775 (2006).
23. M. Armoni, C. Harel, E. Karnieli, GLUT4 goes abnormal: Disregulation of the insulin-responsive glucose transporter in abnormal metabolic states. *Curr. Med. Chem. Immunol. Endocr. Metab. Agents* **5**, 207–217 (2005).
24. M. Gaster, P. Staehr, H. Beck-Nielsen, H. D. Schrøder, A. Handberg, GLUT4 is reduced in slow muscle fibers of type 2 diabetic patients: Is insulin resistance in type 2 diabetes a slow, type 1 fiber disease? *Diabetes* **50**, 1324–1329 (2001).
25. U. Kampmann, B. Christensen, T. S. Nielsen, S. B. Pedersen, L. Ørskov, S. Lund, N. Møller, N. Jessen, GLUT4 and UBC9 protein expression is reduced in muscle from type 2 diabetic patients with severe insulin resistance. *PLOS ONE* **6**, e27854 (2011).
26. M. L. Liu, E. M. Gibbs, S. C. Mccoid, A. J. Milici, H. A. Stukenbrok, R. K. Mcpherson, J. L. Treadway, J. E. Pessin, Transgenic mice expressing the human GLUT4/muscle-fat facilitative glucose transporter protein exhibit efficient glycemic control. *Proc. Natl. Acad. Sci. U.S.A.* **90**, 11346–11350 (1993).
27. B. A. Marshall, M. M. Mueckler, Differential effects of GLUT-1 or GLUT-4 overexpression on insulin responsiveness in transgenic mice. *Am. J. Physiol. Endocrinol. Metab.* **267**, E738–E744 (1994).
28. R. O. Deems, J. L. Evans, R. W. Deacon, C. M. Honer, D. T. Chu, K. Bürki, W. S. Fillers, D. K. Cohen, D. A. Young, Expression of human GLUT4 in mice results in increased insulin action. *Diabetologia* **37**, 1097–1104 (1994).
29. J. M. Ren, B. A. Marshall, M. M. Mueckler, M. McCaleb, J. M. Amatruda, G. I. Shulman, Overexpression of Glut4 protein in muscle increases basal and insulin-stimulated whole body glucose disposal in conscious mice. *J. Clin. Invest.* **95**, 429–432 (1995).
30. A. E. Stenbit, T. S. Tsao, J. Li, R. Burcelin, D. L. Geenen, S. M. Factor, K. Houseknecht, E. B. Katz, M. J. Charron, GLUT4 heterozygous knockout mice develop muscle insulin resistance and diabetes. *Nat. Med.* **3**, 1096–1101 (1997).
31. B. J. Atkinson, B. A. Griesel, C. D. King, M. A. Josey, A. L. Olson, Moderate glut4 overexpression improves insulin sensitivity and fasting triglyceridemia in high-fat diet-fed transgenic mice. *Diabetes* **62**, 2249–2258 (2013).
32. A. Leturque, M. Loizeau, S. Vaulont, M. Salminen, J. Girard, Improvement of insulin action in diabetic transgenic mice selectively overexpressing GLUT4 in skeletal muscle. *Diabetes* **45**, 23–27 (1996).
33. T. S. Tsao, R. Burcelin, E. B. Katz, L. Huang, M. J. Charron, Enhanced insulin action due to targeted GLUT4 overexpression exclusively in muscle. *Diabetes* **45**, 28–36 (1996).
34. A. Zisman, O. D. Peroni, E. D. Abel, M. D. Michael, F. Mauvais-Jarvis, B. B. Lowell, J. F. P. Wojtaszewski, M. F. Hirshman, A. Virkamaki, L. J. Goodyear, C. R. Kahn, B. B. Kahn, Targeted disruption of the glucose transporter 4 selectively in muscle causes insulin resistance and glucose intolerance. *Nat. Med.* **6**, 924–928 (2000).
35. J. K. Kim, A. Zisman, J. J. Fillmore, O. D. Peroni, K. Kotani, P. Perret, H. Zong, J. Dong, C. R. Kahn, B. B. Kahn, G. I. Shulman, Glucose toxicity and the development of diabetes in mice with muscle-specific inactivation of glut4. *J. Clin. Invest.* **108**, 153–160 (2001).
36. A. D. Bach, J. P. Beier, J. Stern-Staeter, R. E. Horch, Skeletal muscle tissue engineering. *J. Cell. Mol. Med.* **8**, 413–422 (2004).
37. M. Juhas, J. Ye, N. Bursac, Design, evaluation, and application of engineered skeletal muscle. *Methods* **99**, 81–90 (2016).
38. Y. Shandalov, D. Egozi, J. Koffler, D. Dado-Rosenfeld, D. Ben-Shimol, A. Freiman, E. Shor, A. Kabala, S. Levenberg, An engineered muscle flap for reconstruction of large soft tissue defects. *Proc. Natl. Acad. Sci. U.S.A.* **111**, 6010–6015 (2014).
39. M. T. Li, M. A. Ruehle, H. Y. Stevens, N. Servies, N. J. Willett, S. Karthikeyakannan, G. L. Warren, R. E. Guldberg, L. Krishnan, Skeletal myoblast-seeded vascularized tissue

scaffolds in the treatment of a large volumetric muscle defect in the rat biceps femoris muscle. *Tissue Eng. Part A* **23**, 989–1000 (2017).
40. S. Brookes, S. Voytik-Harbin, H. Zhang, S. Halum, Three-dimensional tissue-engineered skeletal muscle for laryngeal reconstruction. *Laryngoscope* **128**, 603–609 (2018).
41. L. Perry, S. Landau, M. Y. Flugelman, S. Levenberg, Genetically engineered human muscle transplant enhances murine host neovascularization and myogenesis. *Commun. Biol.* **1**, 161 (2018).
42. T. Kaufman, B. Kaplan, L. Perry, Y. Shandalov, S. Landau, I. Srugo, D. Ad-El, S. Levenberg, Innervation of an engineered muscle graft for reconstruction of muscle defects. *Am. J. Transplant.* **19**, 37–47 (2019).
43. C. Huang, R. Somwar, N. Patel, W. Niu, D. Török, A. Klip, Sustained exposure of L6 myotubes to high glucose and insulin decreases insulin-stimulated GLUT4 translocation but upregulates GLUT4 activity. *Diabetes* **51**, 2090–2098 (2002).
44. W. Niu, P. J. Bilan, S. Ishikura, J. D. Schertzer, A. Contreras-Ferrat, Z. Fu, J. Liu, S. Boguslavsky, K. P. Foley, Z. Liu, J. Li, G. Chu, T. Panakkezhum, G. D. Lopaschuk, S. Lavandero, Z. Yao, A. Klip, Contraction-related stimuli regulate GLUT4 traffic in C2C 12-GLUT4myc skeletal muscle cells. *Am. J. Physiol. Endocrinol. Metab.* **298**, E1058–E1071 (2010).
45. T. Fujimoto, K. Sugimoto, T. Takahashi, Y. Yasunobe, K. Xie, M. Tanaka, Y. Ohnishi, S. Yoshida, H. Kurinami, H. Akasaka, Y. Takami, Y. Takeya, K. Yamamoto, H. Rakugi, Overexpression of Interleukin-15 exhibits improved glucose tolerance and promotes GLUT4 translocation via AMP-Activated protein kinase pathway in skeletal muscle. *Biochem. Biophys. Res. Commun.* **509**, 994–1000 (2019).
46. B. K. Pedersen, M. A. Febbraio, Muscle as an endocrine organ: Focus on muscle-derived interleukin-6. *Physiol. Rev.* **88**, 1379–1406 (2008).
47. S. I. Ikeda, Y. Tamura, S. Kakehi, H. Sanada, R. Kawamori, H. Watada, Exercise-induced increase in IL-6 level enhances GLUT4 expression and insulin sensitivity in mouse skeletal muscle. *Biochem. Biophys. Res. Commun.* **473**, 947–952 (2016).
48. A. K. Linnemann, J. Blumer, M. R. Marasco, T. J. Battiola, H. M. Umhoefer, J. Y. Han, D. W. Lamming, D. B. Davis, Interleukin 6 protects pancreatic β cells from apoptosis by stimulation of autophagy. *FASEB J.* **31**, 4140–4152 (2017).
49. E. G. Hong, J. K. Hwi, Y.-R. Cho, H. J. Kim, Z. Ma, T. Y. Yu, R. H. Friedline, E. Kurt-Jones, R. Finberg, M. A. Fischer, E. L. Granger, C. C. Norbury, S. D. Hauschka, W. M. Philbrick, C.-G. Lee, J. A. Elias, J. K. Kim, Interleukin-10 prevents diet-induced insulin resistance by attenuating macrophage and cytokine response in skeletal muscle. *Diabetes* **58**, 2525–2535 (2009).
50. S. Dagdeviren, D. Y. Jung, E. Lee, R. H. Friedline, H. L. Noh, J. H. Kim, P. R. Patel, N. Tsitsilianos, A. V. Tsitsilianos, D. A. Tran, G. H. Tsougranis, C. C. Kearns, C. P. Uong, J. Y. Kwon, W. Muller, K. W. Lee, J. K. Kim, Altered interleukin-10 signaling in skeletal muscle regulates obesity-mediated inflammation and insulin resistance. *Mol. Cell. Biol.* **36**, 2956–2966 (2016).
51. L. Q. Jiang, N. Franck, B. Egan, R. J. O. Sjögren, M. Katayama, D. Duque-Guimaraes, P. Arner, J. R. Zierath, A. Krook, Autocrine role of interleukin-13 on skeletal muscle glucose metabolism in type 2 diabetic patients involves microRNA let-7. *Am. J. Physiol. Endocrinol. Metab.* **305**, E1359–E1366 (2013).
52. P. Darkhal, M. Gao, Y. Ma, D. Liu, Blocking high-fat diet-induced obesity, insulin resistance and fatty liver by overexpression of Il-13 gene in mice. *Int. J. Obes.* **39**, 1292–1299 (2015).
53. A. Fodor, E. Karnieli, Challenges of implementing personalized (precision) medicine: A focus on diabetes. *Per. Med.* **13**, 485–497 (2016).
54. S. Dimauro, H. O. Akman, C. Paradas, in *Neuromuscular Disorders in Clinical Practice* (Springer New York, 2014); http://link-springer-com-443.webvpn.fjmu.edu.cn/chapter/10.1007/978-1-4614-6567-6_63, vol. 9781461465676, pp. 1311–1334.
55. C. Angelini, C. Semplicini, Metabolic myopathies: The challenge of new treatments. *Curr. Opin. Pharmacol.* **10**, 338–345 (2010).
56. F. M. Platt, A. d'Azzo, B. L. Davidson, E. F. Neufeld, C. J. Tifft, Lysosomal storage diseases. *Nat. Rev. Dis. Primers* **4**, 27 (2018).
57. A. Lesman, J. Koffler, R. Atlas, Y. J. Blinder, Z. Kam, S. Levenberg, Engineering vessel-like networks within multicellular fibrin-based constructs. *Biomaterials* **32**, 7856–7869 (2011).
58. J. Koffler, K. Kaufman-Francis, S. Yulia, E. Dana, A. P. Daria, A. Landesberg, S. Levenberg, Improved vascular organization enhances functional integration of engineered skeletal muscle grafts. *Proc. Natl. Acad. Sci. U.S.A.* **108**, 14789–14794 (2011).
59. A. Ueyama, K. L. Yaworsky, Q. Wang, Y. Ebina, A. Klip, GLUT-4myc ectopic expression in L6 myoblasts generates a GLUT-4-specific pool conferring insulin sensitivity. *Am. J. Physiol. Endocrinol. Metab.* **277**, E572–E578 (1999).
60. F. Kanai, Y. Nishioka, H. Hayashi, S. Kamohara, M. Todaka, Y. Ebina, Direct demonstration of insulin-induced GLUT4 translocation to the surface of intact cells by insertion of a c-myc epitope into an exofacial GLUT4 domain. *J. Biol. Chem.* **268**, 14523–14526 (1993).
61. M. Armoni, M. J. Quon, G. Maor, S. Avigad, D. N. Shapiro, C. Harel, D. Esposito, Y. Goshen, I. Yaniv, E. Karnieli, PAX3/forkhead homolog in rhabdomyosarcoma oncoprotein activates glucose transporter 4 gene expression in vivo and in vitro. *J. Clin. Endocrinol. Metab.* **87**, 5312–5324 (2002).
62. A. M. Fernández, J. K. Kim, S. Yakar, J. Dupont, C. Hernandez-Sanchez, A. L. Castle, J. Filmore, G. I. Shulman, D. Le Roith, Functional inactivation of the IGF-I and insulin receptors in skeletal muscle causes type 2 diabetes. *Genes Dev.* **15**, 1926–1934 (2001).
63. C. Trapnell, L. Pachter, S. L. Salzberg, TopHat: Discovering splice junctions with RNA-Seq. *Bioinformatics* **25**, 1105–1111 (2009).
64. S. Anders, P. T. Pyl, W. Huber, HTSeq—A Python framework to work with high-throughput sequencing data. *Bioinformatics* **31**, 166–169 (2015).
65. M. I. Love, W. Huber, S. Anders, Moderated estimation of fold change and dispersion for RNA-seq data with DESeq2. *Genome Biol.* **15**, 550 (2014).
66. S. Babicki, D. Arndt, A. Marcu, Y. Liang, J. R. Grant, A. Maciejewski, D. S. Wishart, Heatmapper: Web-enabled heat mapping for all. *Nucleic Acids Res.* **44**, W147–W153 (2016).
67. E. Eden, D. Lipson, S. Yogev, Z. Yakhini, Discovering motifs in ranked lists of DNA sequences. *PLOS Comput. Biol.* **3**, e39 (2007).
68. E. Eden, R. Navon, I. Steinfeld, D. Lipson, Z. Yakhini, *GOrilla*: A tool for discovery and visualization of enriched GO terms in ranked gene lists. *BMC Bioinformatics.* **10**, 48 (2009).
69. D. Szklarczyk, A. L. Gable, D. Lyon, A. Junge, S. Wyder, J. Huerta-Cepas, M. Simonovic, N. T. Doncheva, J. H. Morris, P. Bork, L. J. Jensen, C. Von Mering, STRING v11: Protein-protein association networks with increased coverage, supporting functional discovery in genome-wide experimental datasets. *Nucleic Acids Res.* **47**, D607–D613 (2019).
70. J. Cox, M. Y. Hein, C. A. Luber, I. Paron, N. Nagaraj, M. Mann, Accurate proteome-wide label-free quantification by delayed normalization and maximal peptide ratio extraction, termed MaxLFQ. *Mol. Cell. Proteomics* **13**, 2513–2526 (2014).
71. S. Tyanova, T. Temu, P. Sinitcyn, A. Carlson, M. Y. Hein, T. Geiger, M. Mann, J. Cox, The Perseus computational platform for comprehensive analysis of (prote)omics data. *Nat. Methods* **13**, 731–740 (2016).

Acknowledgments: We would like to thank J. Zavin for assistance with staining and cryosectioning, O. Karni-Katovitch for assistance with imaging, and M. Armoni for advice in the early stages of the study. We also thank the Technion's Preclinical Research Authority and M. Tendler for professional animal care; D. Safina for editorial assistance with the preparation of this manuscript; the "Technion Genome Center" for sequencing, quality control, and initial bioinformatic analyses; and the Technion's "Smoler Proteomics Center" for support with proteome measurements and analysis. M.B. would also like to thank the support of the Ariane de Rothschild Women Doctoral Program of the Rothschild Caesarea Foundation. **Funding:** This work was funded by The Rina and Avner Schneur Center of Diabetes Research and in part by Linda Rose Diamond fund for diabetes research. This work was also supported by National Cancer Institute grant K08CA190770 to E.J.G. and grant R01CA128799 to D.L. **Author contributions:** E.K., E.C.L., and S.L. conceived the study idea. M.B., E.K., and S.L. designed the experiments. M.B., C.H., and I.M. performed the experiments. P.J.B. and A.K. created the L6 overexpressing cell line and the GLUT4 pQCXIB retroviral plasmid. E.J.G. and D.L. created the $Rag1^{-/-}$/MKR mouse model. M.B., E.K., and S.L. analyzed the data. M.B., E.K., and S.L. wrote the manuscript. All authors read and approved the final manuscript. **Competing interests:** S.L., E.K., E.C.L., M.B., and C.H. are inventors on a patent, "Methods and compositions for treating and preventing diabetes"/US16/967,237/PENDING PATENT related to this work filed jointly by the Technion and Ben Gurion University on 4 February 2019. The authors declare no other competing interests. **Data and materials availability:** All data needed to evaluate the conclusions in the paper are present in the paper and/or the Supplementary Materials.

Submitted 3 January 2021
Accepted 23 August 2021
Published 13 October 2021
10.1126/sciadv.abg3947

Citation: M. Beckerman, C. Harel, I. Michael, A. Klip, P. J. Bilan, E. J. Gallagher, D. LeRoith, E. C. Lewis, E. Karnieli, S. Levenberg, GLUT4 overexpressing engineered muscle constructs as a therapeutic platform to normalize glycemia in diabetic mice. *Sci. Adv.* **7**, eabg3947 (2021).